Manuscript JPV-2021-06-0245-PVSC, submitted to IEEE Journal of Photovoltaics (special issue for IEEE PVSC 2021 conference)

A Comparison of Emerging Non-Fluoropolymer-Based Co-Extruded PV Backsheets to Industry-Benchmark Technologies

Michael Thuis[1], Naila M. Al Hasan[1], Rachael L. Arnold[1], Bruce King[2], Ashley Maes[2], David C. Miller[1], Jimmy M. Newkirk[1], Laura T. Schelhas[1], Archana Sinha[3], Kent Terwilliger[1], Soňa Uličná[3], and Kurt Van Durme[4]

[1] *National Renewable Energy Laboratory, Golden, CO, 80401, USA*

[2] *Sandia National Laboratories, Albuquerque, NM, 87123, USA*

[3] *SLAC National Accelerator Laboratory, Menlo Park, CA, 94025, USA*

[4] *Endurans Solar Solutions B.V., Geleen, 6167, NL*

***Abstract*—As the photovoltaic (PV) industry is rapidly expanding around the world, there has been an increasing interest in extending the lifespan of PV modules. Concern has also emerged regarding the recyclability of modules and their component materials, including fluoropolymer-based backsheets. Laminated polyethylene-terephthalate (PET) core backsheets have traditionally been used in the PV industry, but new, co-extruded polyolefin (PO) backsheets show promise as an improved alternative. Mini-module and coupon samples of seven different backsheets (made of layers including contemporary PET and fluoropolymers, novel PO, and polyamide (PA) materials) were run through hygrometric- or UV photolytic-accelerated aging to identify and better understand each material's degradation modes and the backsheets' field reliability. In addition to the artificial aging, the natural weathering methods used in this study are described. The comprehensive set of chemical, mechanical, and structural characterizations at intermittent read points in this study is presented, including: visual appearance and color; gloss; mechanical tensile testing; I-V performance; electroluminescence (EL) imaging; dielectric breakdown; FTIR-chemical structure; X-ray-polymer structure (WAXS); and DSC-crystalline content. After 4000 h of aging, a strong correlation occurs between initial physical characteristics (mechanical tensile test) and operating performance (EL and I-V characteristics).**

Keywords—backsheet, damp heat testing, durability, DuraMAT, IEC TS 62788-7-2, PET, polyolefin, UV weathering

I. Background and Introduction

Photovoltaic (PV) modules are designed as multilayered, composite systems consisting of glass, polymeric (encapsulant and backsheet), semiconductor, and metallic components. Polymeric backsheets are critical to the overall performance and lifespan of contemporary module designs. The backsheet serves as a packaging material, protecting the electrical components of the module against shunting and fire ignition, so it must be resilient in a variety of meteorological climates. Polyethylene-based backsheet materials, including an electrically insulating biaxially oriented polyethylene-terephthalate (PET) core, have been commonly used in the PV industry for decades. Traditional backsheets consist of laminates of two or more layers (which may include an adhesive) with an intended orientation of use (air- or sun-facing surfaces). A fluoropolymer layer may be added to PET to improve durability in the natural environment. Fluoropolymers are, however, difficult to recycle or decompose—which may prevent the recovery and reuse of valuable components at the end of the module service life. Field inspections of PV installations have shown that both traditional and more recent backsheets are vulnerable to embrittlement (cracking) and delamination, compromising essential relied upon insulation (RUI) in the PV module [1]. These degradation modes present an immediate safety concern to workers maintaining PV systems in addition to causing losses in performance (through tripped inverters, corrosion, and other degradation) [2]. Recent research into polyolefin (PO)-based backsheets has shown promising robustness relative to present PET-based backsheet materials, suggesting they may be used to extend the lifespan of PV modules [3]. PO backsheets may be co-extruded, reducing the cost of fabrication and the risk of delamination. Furthermore, polyolefins may be formulated to be environmentally robust, such that no fluoropolymer outer layer is needed.

This study investigates emerging PO-based backsheets, comparing their durability to existing, PV industry benchmark products in a comprehensive aging study. This study is also known as the "Comparison of market-benchmark BACKsheet technologies to novel non-FLuoro-based co-extruded materials and their correlation and ImPact on PV module degradation

rates" (BACKFLIP) study. Photolytic- and hygrometric-accelerated testing are applied to both coupon and mini-module (MiMo) specimens to identify and understand the different degradation modes of the backsheets. Characteristics related to appearance, mechanical performance, electrical performance, crystalline-structure and -content, and polymer chemical structure will be correlated between the accelerated tests to develop degradation models. The artificial aging and models will also be validated relative to natural weathering experiments in Albuquerque, NM, and Cocoa, FL. Artificial and natural aging will be compared to identify the characteristics that may be used to best monitor degradation and predict durability.

II. Experimental

A. Test Specimens and Specimen Fabrication

TABLE I. BACKSHEET PRODUCTS USED IN THIS STUDY

Arbitrary Index	Backsheet	Total Thickness, [AVG ± 2 S.D.] (mm)	Comment
BS-1	PO-1	0.35 ± 0.01	In Development
BS-2	PO-2	0.35 ± 0.02	In Development
BS-3	TPT	0.32 ± 0.01	Traditional (Reference)
BS-4	APO	0.35 ± 0.01	Recently Developed
BS-5	PPE	0.36 ± 0.01	Contemporary
BS-6	AAA	0.33 ± 0.02	Known Bad
BS-7	KPf	0.29 ± 0.00	Contemporary

Polymer sheet coupons and MiMos were manufactured using seven different backsheets, as presented in Table I. The backsheets for the study included three benchmark products (TPT, PPE, and KPf); one known bad backsheet (AAA); and three novel polyolefin backsheets (PO-1, PO-2, and APO). TPT consists of laminated PVF/PET/PVF, where "PVF" indicates polyvinyl fluoride layers; PPE is laminated pigmented PET/unpigmented PET/EVA, where "EVA" is poly(ethylene-co-vinyl acetate); and KPf is laminated polyvinylidene fluoride (PVDF)/PET/fluorinated coating. AAA is a recent co-extruded backsheet composed of polyamide (PA)/blended PA and polypropylene (PP)/PA layers. The aforementioned polymers are formulated with additives (which may include UV absorbers, UV stabilizers, and antioxidants), sometimes in addition to mechanical reinforcers and/or fillers. The MiMos were manufactured using non-tempered float glass (Planibel Clearvision, AGC Inc.) with no anti-reflective coating. A single 156-mm, stabilized Si-Cz, p-type passivated emitter and rear cell (p-PERC, previously diced into four equal pieces) was connected with ribbon to an edge-mounted junction box equipped with removable MC4, UTX end connectorized cables. EVA encapsulant, including a UV transparent front layer and a UV blocking rear layer, was laminated to attach the MiMo components. Coupon specimens consisted of polymer backsheet that was run through the same lamination process to give the same thermal history as the MiMos. The MiMos were subsequently outdoor light-soaked (to mitigate light-induced degradation of the cells [4]) and then verified using electroluminescence (EL) imaging and current-voltage (I-V) measurements. A subset of MiMos was examined at the National Renewable Energy Laboratory (NREL) to verify that light enhanced thermal-induced degradation [5] was ≤ 1% of the maximum power after 1 week of IEC TS 62788-7-2 method A3 [6] and UV-light-induced degradation of the cells was ≤ 1.4% of the maximum power after 4 weeks of UV weathering in a UVA-340 chamber [7]. This was a partially blind study where all samples were initially tested as unknown materials with an arbitrary index, and each specimen had a serial number.

B. Accelerated Testing

Test samples were weathered using seven different accelerated test conditions, summarized in Table II. Xenon-arc test chambers (Ci5000 Weather-Ometer, Atlas Material Testing Technology LLC) were used for UV weathering. Coupons and MiMo specimens were mounted with the air side facing towards the Xe lamp. Separate combined temperature/humidity chambers (e.g., BTX-475, ESPEC North America Inc.) were used for hygrometric weathering. The surface temperature of the MiMos and coupons in the chamber was verified for the sample sun side using T-type thermocouples with a wireless transmitter (MWTC-D-T-915, Omega Engineering Inc.) through 90 minutes of aging. The nominal relative humidity (RH) setting is given for each of the experiments in Table II. Weathering was performed at read points of 0, 1000, 2000, 3000, and 4000 hours cumulative duration.

TABLE II. ACCELERATED TESTING CONDITIONS

Arbitrary Experiment Index	UV Irradiance ($W \cdot m^{-2}$ at 340 nm)	MiMo Temperature (°C)	Chamber Relative Humidity (%)	Water Spray?	Ref.
1	0	85	85%	N	[8]
2	0	65	85%	N	N/A
3	0	45	85%	N	N/A
a (A3)	0.80	69	20%	N	[6]
b	0.55	59	20%	N	N/A
c	0.55	61	~80%	Y	N/A
d (A2)	0.80	59	20%	N	[6]

C. Characterization Methods

In this study, MiMo and coupon samples were characterized for color (i.e., L, a*, and b*, using a CM-700d Portable Spectrophotometer, Konica Minolta Inc.); gloss (for 20°, 60°, and 85° [9], using a micro-TRI-gloss meter, BYK-Gardner GmbH); visual appearance (α99 MII digital camera, Sony Corp.); optical microscopy (VHX 5000 digital microscope, Keyence Corp.); wide-angle X-ray scattering (WAXS) of the polymer structure (Stanford Synchrotron Radiation Lightsource, SSRL) [10]; and Fourier-Transform Infrared (FTIR) chemical structure (Alpha-II spectrometer with "Pt" ATR Fixture, Bruker Corp). In this study, the electrical performance of the MiMos was characterized using I-V flash testing (at 1000 $W \cdot m^{-2}$ using a 5600 Solar Simulator, Eternalsun Spire) followed by EL imaging (Proline IR Camera, Finger Lakes Instrumentation and an N5768A DS power supply,

Agilent Technologies Inc.). Destructive characterization including mechanical tensile testing (1122/5500R tensile tester with Automatic Video Extensometer attachment, Instron Corp.); DC breakdown voltage (4TCE100-10/D149 tester, Phenix Technologies Inc.) [11]; and differential scanning calorimetry (DSC) of the crystalline content (Q2000 equipped with RCS 90 refrigerating unit, TA Instruments-Waters LLC) were conducted after cutting the coupons into smaller specimens [10]. Of the aforementioned characterizations used for the study, this paper will focus on mechanical tensile test, EL imaging, optical microscopy, and FTIR.

III. Results and Discussion

A. Initial Mechanical Performance of the Backsheets

The mechanical performance of the backsheets before aging is shown in Fig. 1. Data curves for each backsheet represent the median of the five replicate specimens examined, with the tensile axis aligned to the transverse direction (TD) during fabrication. The stress is indicated relative to the original specimen thickness in Table I. Distinct stress/strain profiles are observed for the backsheets, including PET-based (which have the greatest ultimate tensile strength), PA-based (which have a limited maximum stress and strain), and PO-based (which have the greatest elongation to break).

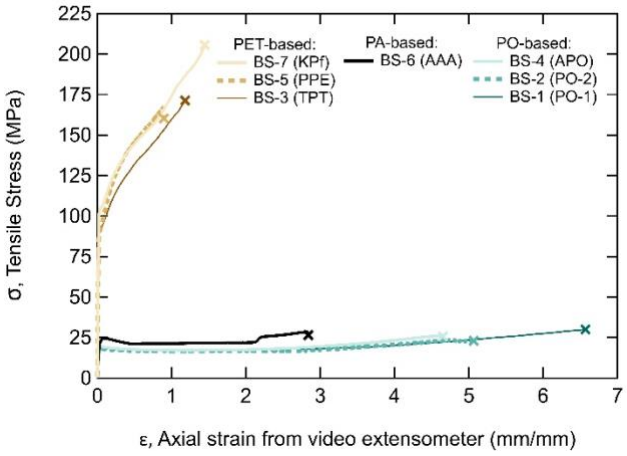

Fig. 1. Representative stress/strain profiles for unaged backsheets along the TD. The backsheets are grouped by the composition of their component layers.

Regarding Fig. 1, the differences in mechanical performance between the groups of backsheets result from their component layers. PET is a mechanically stiff and tough layer that dominates the mechanical response of BS-3, BS-5, and BS-7 because it is the thickest layer in those backsheets and is also biaxially oriented. In comparison, the present manufacturing process does not allow the PO core layer in BS-1, BS-2, and BS-4 to be biaxially oriented. The PO layers in BS-1, BS-2, and BS-4 are lower density and more compliant, allowing for elongation. The core of BS-6 is mechanically reinforced by randomly oriented glass fibers [12]. The backsheets are readily distinguished into the groups in Fig. 1 based on their chemical structure (FTIR), polymer structure (WAXS), and phase transition temperature (DSC) [10].

B. Electrical Performance of the Mini-Modules

The electrical performance of MiMo specimens is qualitatively compared in Fig. 2 in EL images from the beginning through the end of the 85°C/85% RH damp heat (DH) experiment. One backsheet from each of the composition groups in Fig. 1 is shown in Fig. 2: BS-7 for PET-, BS-6 for PA-, and BS-2 for PO-based. MiMo-specific features may be observed through the experiment, including dark regions from broken grid lines (bottom left of BS-2) as well as other fabrication defects. The change in EL intensity contrast in the region adjacent to the busbars is most overt for BS-7 and was similarly observed for BS-3 and BS-5 (not shown). Furthermore, the most substantive changes in BS-7 occur at 3000 h and 4000 h.

The backsheet-specific performance of the groups identified in Fig. 1 is quantitatively distinguished with aging in the I-V performance of the MiMos, and is attributed to the characteristics of component layers of the backsheets. Distinct backsheet-specific durability is observed in the unique specimen geometry specific to this study (¼ cell MiMos). While the results in Fig. 2 are shown for hygrometric aging, the MiMo geometry examined here importantly allows for UV weathering in a xenon-arc test chamber, where high spectral fidelity relative to the terrestrial sun can be achieved.

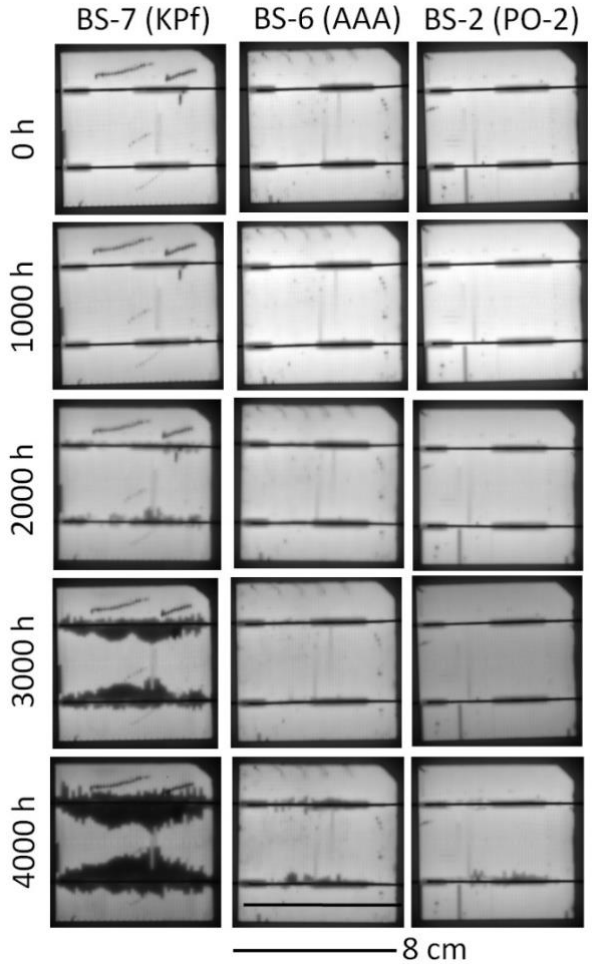

Fig. 2. Representative EL images of the MiMos through hygrometric aging (85ºC/85% RH). One backsheet of each type (BS-7: PET, BS-6: AAA, and BS-2: PO) is shown.

The effect of the experimental conditions in Table II on the quantitative MiMo electrical performance is summarized in Fig. 3. The figure shows the maximum power (P_{max}) averaged for all seven backsheets at each read point. The change in P_{max} is shown relative to the measurements for the unaged MiMos. Data are connected in Fig. 3 with lines to guide the eye; no model or other assumptions are used for the lines in the figure. A decrease in P_{max} is seen with increased exposure time for all hygrometric test conditions, where the order of severity (greatest to least) is given by 1 (85°C/85% RH), then 2 (65°C/85% RH), and then 3 (45°C/85% RH). On the other hand, an increase in performance is seen for the a (A3) and d (A2) experiments through 2000 h (shown in Fig. 3), with a corresponding increase in the open-circuit voltage (V_{oc}) and short-circuit current (I_{sc}) [13]. The I_{sc} (both unaged and through aging) for BS-3, BS-5, and BS-7 was less than all other backsheets in all experiments [13].

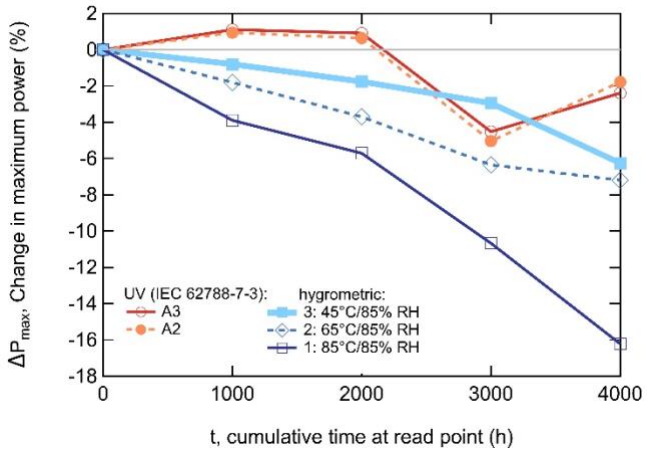

Fig. 3. Evolution of the maximum power through accelerated testing, averaged at each read point for all backsheets in each experiment.

Fig. 3 shows that the hygrometric tests are the most damaging to PV performance, with 85°C/85% RH being the most damaging experiment. A comparison of Fig. 2 and Fig. 3 identifies that loss of power results from degradation, including corrosion of interconnects (i.e., the bus bars, solder, and ribbons). The increase in power for UV weathering may result from corrosion of the front glass surface, a phenomenon which has recently been verified outside of this study from optical and electron microscopy of the surfaces of soda-lime glass following the A3 test condition. Glass corrosion is known to give an antireflective effect [14], which would increase I_{sc} and P_{max}. The effect of glass corrosion, however, eventually becomes detrimental with prolonged stress testing, i.e., beyond the 2000 h in Fig. 3. The decrease in I_{sc} for PET-based backsheets (BS-3, BS-5, and BS-7) may follow from the optical performance of backsheet additives (including pigments, UV blockers, and fillers) in those backsheets.

The changes in P_{max} and the series resistance (R_{series}) with aging are examined in Fig. 4 and Fig. 5, respectively, for each backsheet material in the 85°C/85% RH experiment. Data points are connected in the figures strictly to guide the eye. A loss in power is observed for all backsheets. The trend is similar through 2000 h, and BS-3, BS-5, and BS-7 are then most affected through 4000 h. While P_{max} is shown in Fig. 4, I_{sc} was reduced ~3x relative to V_{oc} through the 85°C/85% RH aging [13]. R_{series} generally increases through DH for all the backsheets, as shown in Fig. 5. A steeper inflection, however, is observed in the figure for BS-3, BS-5, and BS-7. On the other hand, there is no clear trend for shunt resistance (R_{shunt}) until 2000 h, beyond which a noticeable decrease in R_{shunt} is observed for BS-3, BS-5, and BS-7 with DH [13].

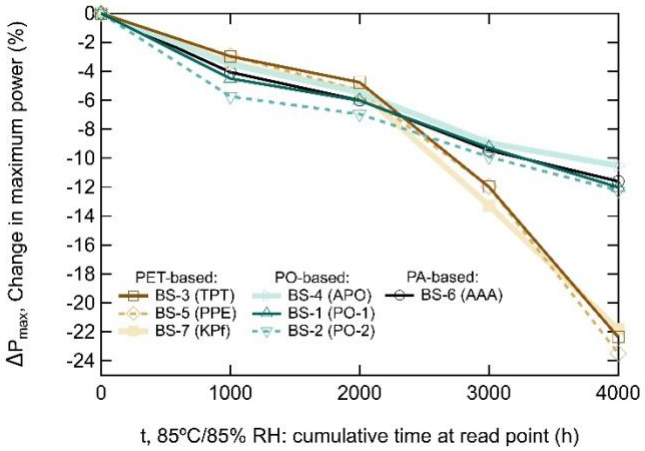

Fig. 4. Evolution of P_{max} in experiment 1 (85°C/85% RH) for the seven backsheet products examined in this study.

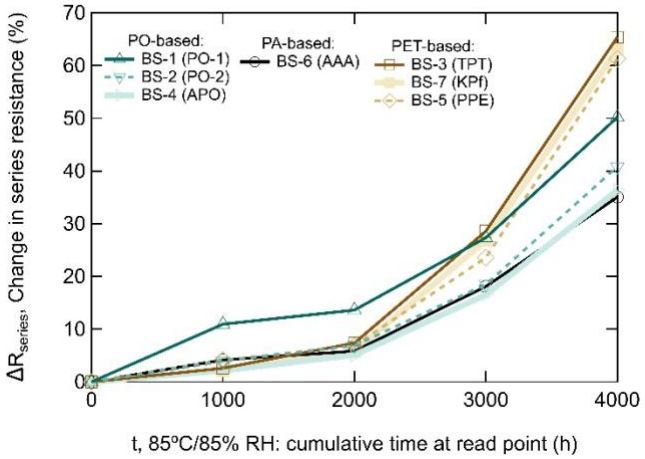

Fig. 5. Evolution of R_{series} in experiment 1 (85°C/85% RH) for the seven backsheet products examined in this study.

In Fig. 4 and Fig. 5, a similar grouping of backsheets is observed as in Fig. 1, including BS-3, BS-5, and BS-7 (which have the greatest reductions in P_{max}). The non-PET-based backsheets (BS-1, BS-2, BS-4, and BS-6) are not as obviously distinguished, however. The greatest damage for the PET-based backsheets (BS-3, BS-5, and BS-7) is seen starting at 2000 h, as shown in Fig. 2. The greater change in the laminated PET-based backsheets may come from hydrolysis of the core layer. For PET, hydrolysis can generate acid species (e.g., terephthalic acid), which may directly affect metallic interconnects and/or catalyze the degradation of EVA—which can also generate acidic species (e.g., acetic acid). Acidic species may corrode the metals present in the interconnects; they may also catalyze the degradation of backsheet layers [15], [16]. The backsheets have

different rates of acid transmission, which may also affect the extent of corrosion. Loss in I_{sc} is consistent with increased series resistance from corrosion, qualitatively observed in Fig. 2 and quantified in Fig. 5. Separately, the formation of intermetallic compounds has been observed in modules used in hot and humid locations [17], which may be limited in this study because the MiMos were aged in an open circuit electrical bias. Loss in V_{oc} and increase in R_{shunt} may result from damage to the cell. Fig. 2, Fig. 4, and Fig. 5 confirm that backsheets are able to protect the front of the cell, presumably based on the diffusivity and mass transport characteristics of the different backsheet materials as well as their electrical insulation. The figures further confirm that the ¼ cell MiMo construction is helpful in distinguishing module components, which is particularly beneficial for UV weathering (where chamber space is expensive).

C. Examination of Surface Damage to the Backsheets

The examination of surface integrity from optical microscopy of the air side of select MiMos is summarized in Fig. 6. The detail for BS-1, BS-2, BS-4, BS-5, and BS-6 is compared at the same scale, with additional images given at greater magnification for BS-6. Representative images are compared between unaged specimens as well as after 4000 h cumulative for the 85°C/85% RH and the A3 tests. The color contrast between the images of the same backsheets results from subtle differences in imaging, including the use of cross-polarizers between imaging sessions. Fig. 6 shows micro-scale cracks extending in both the machine extrusion and transverse directions for BS-4 and BS-6 (after the A3 experiment) as well as for BS-2 after aging at 85°C/85% RH. In coupons, micro-cracking was only observed for the air side of BS-4 (not shown), which was less developed than in the MiMos. Fig. 6 shows a less connected network of even smaller surface cracks for BS-6 after the 85°C/85% RH test. These incipient cracks were observed in select regions in the center of the MiMo, and were also observed throughout the air- and sun-sides of the BS-6 coupons after the 85°C/85% RH test [13]. Localized cracking and loss of the surface layer were observed for BS-5 coupons and MiMos after the 85°C/85% RH test. Fig. 6 shows a crack extending into the PET core layer, with spalling of the surface layer along the crack. While the majority of the surface layer remained on BS-5 after the DH test, larger areas of the surface layer were also delaminated, particularly at specimen corners. A scratch is seen in Fig. 6 on the surface of BS-5 (A3 column). While a sparse population of surface scratches, presumably an artifact of specimen handling, were observed on all backsheets, surface scratches are represented in Fig. 6 only for BS-5. Modest differences, in contrast, are observed for BS-1 and BS-2 after A3 weathering.

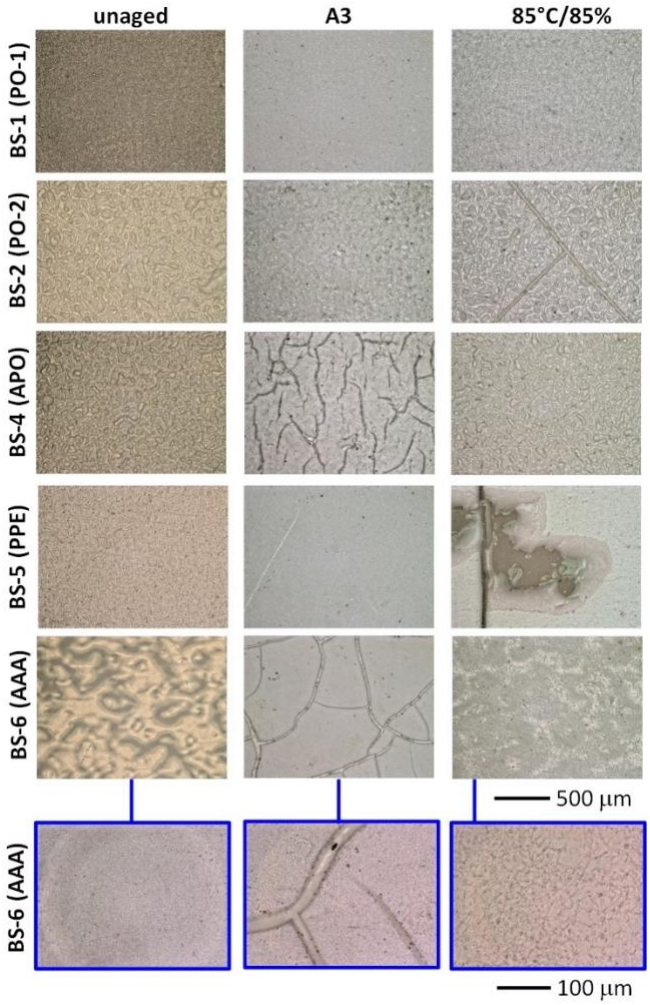

Fig. 6. Microscope images comparing the surface integrity of the air side of select MiMos, unaged as well as after the A3 (4000 h) and 85C/85% RH (4000 h) tests.

Regarding Fig. 6, the change in appearances of BS-1 and BS-2 suggests roughening of the surface from UV weathering. The additional backsheets observed to be cracked in MiMos, as well as the biaxial geometry of the cracks, suggests damage resulting from a misfit strain. Sources of strain may include thermal misfit between components in a multilayer laminate, size change occurring within materials as a result of lamination, and strain from the evolution of crystallinity or change in free volume with aging. The strain between polymer layers in a freestanding coupon sheet would be expected to be less than in a MiMo, because of the very different stiffness of the layers in a MiMo. The existence of a separate incipient crack geometry after 85°C/85% RH suggests different enabling degradation mechanisms may affect BS-6, including UV photodegradation and thermal oxidation. The morphology and implications for BS-6 are consistent with previous examinations of the materials, regarding UV, which may contribute to backsheet cracking [12],[15],[16],[19]. Fig. 6 directly reveals that a separate thermal-degradation must be occurring for BS-6, which is only implied in previous studies. Scratches on any of the backsheets may contribute to cracking, which underscores the need for proper handling before and after lamination. In general, much of

the most ubiquitous damage observed in camera or microscope imaging resulted from UV weathering, thus identifying the importance of photolytic aging in backsheet material selection and module design type qualification.

D. Examination of the Polymer Chemical Structure

The chemistry of BS-6 is compared between experiments and relative to an unaged specimen in Fig. 7. To aid comparison, the spectra have all been normalized relative to the peak at 1465 cm^{-1}. Spectra typically overlap for the hygrometric test conditions as well as the unaged specimen from 4000 cm^{-1} to 800 cm^{-1}. While incipient micro-cracking was observed in microscopy following 85°C/85% RH, no unique features are observed in FTIR characterization. Unique features are, however, observed following UV weathering, including peak broadening about 3282 cm^{-1} and 2912 cm^{-1}; peak enhancement at 1710 cm^{-1} and 1159 cm^{-1}; and peak formation at 1102 cm^{-1}. The features in Fig. 7 were observed on the air side of coupons (facing the lamp) during UV weathering but typically were not observed on the sun side of coupons (facing the chamber walls). At the time of this publication, the MiMos have not yet been fully examined. While the profile shape is self-similar, the intensity is varied between experiments below 800 cm^{-1}. Features similar to BS-6 in Fig. 7 were also observed for BS-4.

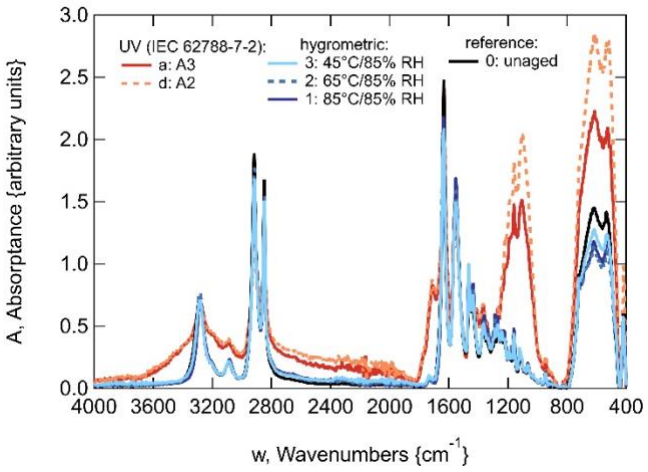

Fig. 7. FTIR spectra for BS-6 (AAA) coupons. The profiles for the air side after 4000 h of aging are shown relative to an unaged specimen.

Peak enhancement and peak formation indicate substantive, molecular changes which can only result from UV photodegradation, as hygrometric weathering was performed in a dark chamber. Peak broadening about ~3200 cm^{-1} was previously attributed to the formation of alcohols and carboxylic acids [18]. The peak at 1710 cm^{-1} was previously attributed to carbonyl group products (i.e., carboxylic acid) resulting from moisture-induced breakdown of imide groups from a photo-oxidation process [12]. The broad peak at 1102 cm^{-1} corresponds to the C-O stretch mode [20] and was previously observed to result from both artificial and natural UV weathering [12]. This peak is attributed to oxidation, i.e. incorporation of C-O moieties into the surface. The UV damage in Fig. 7 occurs with micro-scale mud cracking observed in Fig. 6. The sampling depth for the measurement in Fig. 7, however, is estimated to be on the order of 2 μm because an attenuated total reflectance (ATR) crystal attachment was used in the measurement. A second degradation mechanism (e.g., chain scission, possibly occurring with evolution of the crystallinity) is implied from the spectra for 85°C/85% RH, where no unique features were observed. Thermal degradation might explain the cracking of AAA backsheet during aging at elevated temperatures during relative thermal index testing in the dark [19]. The affects of UV weathering of the known bad BS-6 are also identified in Refs. [12],[15],[16]. Relative to previous studies examining accelerated testing and outdoor weathering, the occurrence of a separate mechanism for thermal-degradation is now directly demonstrated in comparison between Fig. 6 and Fig. 7. Roughening of surface, which facilitates crack formation may also contribute to the incipient features shown in Fig. 6 for 85°C/85% RH. The peaks below 800 cm^{-1} may result from TiO_2 present in the formulation of BS-6, i.e., from fortuitous sampling between measurements or from increased exposure with surface erosion. Practically speaking, the FTIR characterization method may become limited below 600 cm^{-1}. The similar changes observed for BS-4 may result from the polyamide 12 resin also used in the surface layer for that backsheet [10].

Fig. 8 compares the chemistry for BS-5 coupons between experiments and relative to an unaged specimen. As in Fig. 7, the UV weathering experiments are distinguished from the hygrometric experiments and the unaged specimen. After A3 and A2 weathering, the lesser peaks at 2914 cm^{-1}, 2845 cm^{-1}, 2653 cm^{-1}, and 2539 cm^{-1} become subsumed within a stronger but broader peak centered about ~2800 cm^{-1}. Also after A3 and A2, the peak at 1711 cm^{-1} attenuates and shifts to 1677 cm^{-1}. The peaks at 1237 cm^{-1} and 1092 cm^{-1} become attenuated with UV weathering. Lastly, intensification is observed at 667 cm^{-1} for A3 and A2 weathering.

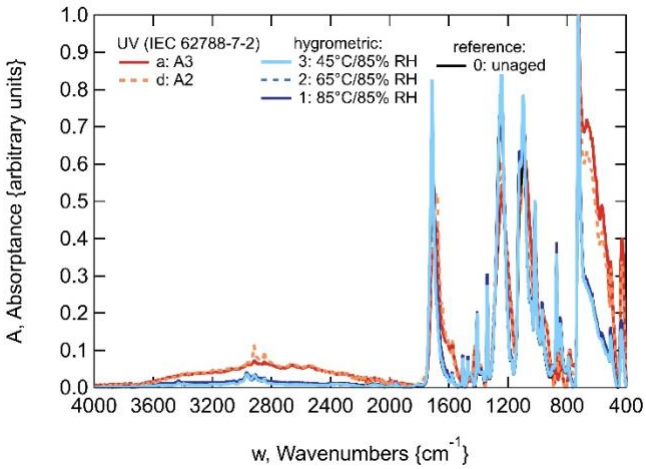

Fig. 8. FTIR spectra for BS-5 (PPE) coupons. The profiles for the air side after 4000 h of aging are shown relative to an unaged specimen.

Activity at 2800 cm^{-1}, 1700 cm^{-1}, and 1150 cm^{-1} corresponds to the stretching modes of the C-H, C=O, and C-O bonds, respectively [20]. As in Fig. 7, these changes are only observed for UV weathering. No surface damage (cracking or delamination), however, is seen for the A3 aged BS-5 specimen in Fig. 6. In contrast, embrittlement of the surface layer is implied in Fig. 6 from the surface damage following DH. The combined observations identify UV photodegradation occurring at the surface of BS-5, with a separate thermal- or hygrometric-

degradation mechanism (possibly occurring with crystallographic evolution) during 85°C/85% RH. Damage to the surface of BS-5 may be compounded by damage to its core layer, which is implied from the cracking and spalling of the core in Fig. 6, as well as the loss of electrical performance shown in Fig. 4. Lastly, increased intensity below 700 cm^{-1} may result from TiO_2 present in the formulation of BS-5, e.g., increased exposure with surface erosion.

Fig. 9 compares the polymer chemical structure for BS-1 MiMo specimens between experiments and relative to an unaged specimen. Primary peaks are observed at 2916 cm^{-1}, 1454 cm^{-1}, 1375 cm^{-1}, 1015 cm^{-1}, and 529 cm^{-1}. No new peaks result from the accelerated tests in this study. Attenuation of the peaks at 2916 cm^{-1} and broadening of the peak above 1015 cm^{-1} is, however, observed after A3 and A2 weathering. The results for MiMo specimens may be compared to those obtained for coupons in Ref. [10]. Increased peak intensity at 3336 cm^{-1}, 1730 cm^{-1}, 1449 cm^{-1}, 1226 cm^{-1}, and 1165 cm^{-1} was observed for the coupons after A3 and A2 weathering.

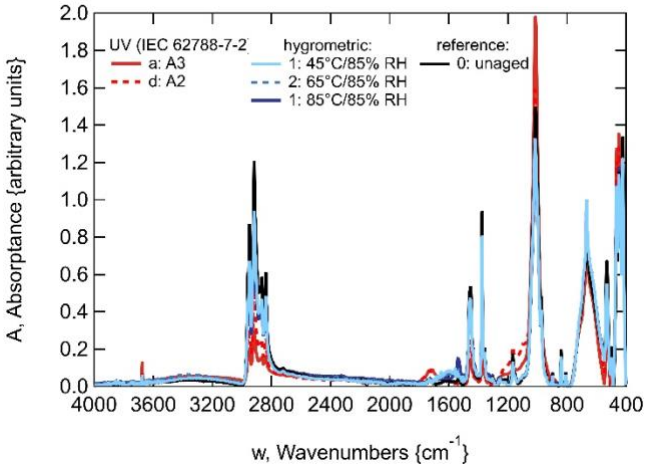

Fig. 9. FTIR spectra for BS-1 (PO-1) MiMo specimens. The profiles for the air side after 4000 h of aging are shown relative to an unaged specimen.

The similar spectra for the MiMo specimens in Fig. 9 suggest the surface of BS-1 is robust relative to the UV and hygrometric stressors used in this study. This is consistent with the lack of surface damage observed in Fig. 6. 1 cm x 3 cm specimens were taken from the MiMos just outside the cell to examine possible interaction with acetic acid, a known by product of the degradation of EVA encapsulant. To explain, this backsheet location is expected to be the most exposed to acid, because the greatest concentration is anticipated between the impermeable cell and front glass layers and a prolonged time duration would occur for acid to diffuse through the thickness of the backsheet or out of the edges of the MiMo. No enhanced degradation, however, is observed for the BS-1 MiMo specimens in Fig. 9 relative to coupons in Ref. [10]. Peak intensification of the BS-1 coupons in Ref. [10] results from additive migration and is not representative of the bulk of the backsheet air side surface layer.

Table III summarizes the results of the ongoing study. Where degradation was observed, the table identifies the associated characterization method; the backsheet(s) affected as well as the enabling material in their core layer (or the backsheet itself); the geometry of affected specimens as well as the affected surface(s) where applicable; and the experiment. Based on Fig. 2, Fig. 3, Fig. 4, and Fig. 5, MiMo performance was most adversely affected for the PET-based backsheets (BS-3, BS-5, and BS-7) in the 85°C/85% RH test condition. Affected characteristics included EL image contrast, P_{max}, R_{series}, and R_{shunt}. BS-5 was also affected in the 85°C/85% RH test condition, including delamination of the surface layer on the air side and embrittlement of the core layer. Based on Fig. 6 and Fig. 7, BS-2, BS-4, BS-5, and BS-6 were affected by UV weathering. Degradation for these backsheets was observed on the irradiated air side of the backsheet. More of the backsheets were observed to be degraded in the MiMo geometry than in coupon specimens. The surface degradation of BS-2 and BS-4 is further described in Ref. [13].

TABLE III. SUMMARY OF RESULTS OF THIS STUDY

CHARACTERIZATION METHOD	BS's AFFECTED (material(s))	SPECIMEN GEOMETRY	EXPERIMENT(S)
I-V	**3, 5, 7** (PET-based)	MiMo	85°C/85% RH
EL	**3, 5, 7** (PET-based)	MiMo	85°C/85% RH
microscope	5 (PPE)	coupon (air side)	85°C/85% RH
microscope	4, 6 (PA-based)	coupon (air side)	A2, A3
microscope	5 (PPE)	MiMo (air side)	85°C/85% RH
microscope	2, 4, 6 (non-PET)	MiMo (air side)	A2, A3
microscope	6 (PA-based)	coupon, MiMo (air side)	85°C/85% RH
FTIR	2, 4, 5, 6	coupon, MiMo (air side)	A2, A3

IV. Discussion

An optimized version of BS-1 is presently commercially available, following after the development of BS-4 then BS-2. BS-4 shows surface cracking in Fig. 6, which may be attributed to UV degradation based on the FTIR spectra in Ref. [13] which are similar to Fig. 7. BS-2 shows surface cracking following 85°C/85% RH in Fig. 6, in additon to UV degradation in the FTIR spectra in Ref. [13]. Unlike BS-4, FTIR confirms the polymer chemical structure of BS-2 is distinctly different from BS-6 or other previous backsheets in this study. BS-1, however does not show micro-scale cracking in Fig. 6 or major changes in peak shape or location in Fig. 9. The robustness of BS-1 to the steady-state UV and hygrometric experiments is encouraging and is presently being validated in this study relative to outdoor locations.

At this point in the study, the connection between surface degradation, bulk degradation, and PV module performance remains to be established for several of the backsheets. Surface damage is traditionally expected to facilitate damage to the bulk in backsheets, which has historically motivated the use of environmentally durable surface layer(s) to protect an insulating core layer. Non-traditional core layers, however, may be more resilient to the PV application environment, and therefore may be more tolerant to surface cracking. The PV industry has recently shifted toward extending the duration of the DH test or even toward the use of more severe pressure cooker tests, both

of which emphasize bulk hydrolysis of PET, but may overlook degradation modes related to backsheet surfaces. Additional clarification may come from the ongoing breakdown voltage and mechanical tensile test characterizations as well as the DSC and X-ray characterizations [10] in this study, all of which examine the bulk characteristics of the backsheet. The ongoing b and c test conditions (Table II) may also provide confirmation and/or further insights related to UV weathering.

This study also reveals the limitations of today's standardized testing. For example, the appropriate duration and even the validity of the DH test remain to be established relative to terrestrial PV installations [21], [22], [23]. Fig. 2 and Fig. 4 suggest that DH testing beyond 2000 h can catastrophically damage PET core layers. A substantial acceleration for the hydrolysis of PET from the DH test has been identified for most terrestrial PV locations [24], i.e., more than 200 years equivalent duration for 2000 h of 85°C/85% RH. The results in Fig. 2 and Fig. 4 immediately seem inapplicable to the PV application given the >30 field history of BS-3, and outdoor weathering in Albuquerque, NM and Cocoa, FL will be used to validate the degradation of the MiMos examined in this study. In comparison, the 65°C/85% RH and 45°C/85% RH test conditions, which more closely approach operating conditions for the PV application, are clearly less damaging in Fig. 2 and Fig. 3. 4000 h of the A3 test condition is generally intended to simulate 5 years of incident UV radiation in hot locations for rack mounted modules with polymers having an activation energy on the order of 50 $kJ \cdot mol^{-1}$. The related characteristic distance for ingress of moisture and oxygen and the corresponding coupon and MiMo specimen size is not yet established. For example, the cracking of the core layer throughout BS-5 specimens suggests the 1 cm edge perimeter used in this study is not sufficient if mass transport of H_2O, O_2, or acid species is of concern. The field validity, appropriate duration, and appropriate specimen size remain to be fully established for the 85°C/85% RH test condition.

The lack of obvious connection between surface- and bulk-degradation in this study may also identify limitations of steady state accelerated testing as well as the characterization methods presently used for backsheets. The connection between surface and bulk may emerge in more extended testing or combined stress testing, or if a test sequence were to be instead used (UV weathering followed by hygrometric testing, thermal cycling, and/or cyclic dynamic mechanical loading). Ultimately, the industry may need more complex accelerated tests than the steady-state conditions examined in this study to better represent the PV application environment. This study will separately advise on the characteristics and characterization methods used with PV backsheets. Discoloration need not be correlated with mechanical performance or electrical insulation. Likewise, surface cracking may not automatically compromise photovoltaic performance or electrical RUI. The correlation and identification of the most critical characteristics as well as the further development of characterization methods remain to be studied in the PV industry. The need for continued improvement of the accelerated tests, specimen standardization, and characterization methods is evident from the BACKFLIP study.

V. Summary

The BACKFLIP study is an ongoing empirical examination of the durability of photovoltaic backsheets. Key results include the following:

- Groups of backsheets are readily distinguished in the results of unaged samples and after accelerated testing, including laminated PET-core, co-extruded PO-core, and AAA products.
- Changes in electrical performance of MiMos, degradation of the backsheet surface, and degradation of the bulk of the backsheet are distinguished between the samples examined. The distinct results confirm the use of the ¼-cell MiMo design for high-spectral-fidelity UV weathering and hygrometric testing.
- The observed degradation of the backsheets is consistent with the hydrolysis of the bulk (core) layers or photodegradation of the surfaces. The connection between bulk- and surface-degradation, however, remains to be established (if it exists) in the ongoing characterizations and experiments in the study.
- In addition to guidance on the materials used, the BACKFLIP study is expected to advise on the accelerated tests and characterization methods used with PV backsheets. For example, PET-core based backsheets became extensively damaged after 2000 h of damp heat, raising concerns regarding the field validity and appropriate duration for the 85°C/85% RH test condition. Separately, the connection between surface and bulk may emerge in more extended testing or combined stress testing, or if a test sequence were to be used instead.

Acknowledgments

The authors would like to thank BACKFLIP contributors, including Allen Anderberg, Paul Ndione, Greg Perrin (NREL); Frederic Dross, Robert Janssen, Sven Kresig, Milica Mrcarica, Peter Pasmans, Nicola Sicchieri, and Nicoleta Voicu (DSM). Funding was provided as part of the Durable Modules Consortium (DuraMAT), an Energy Materials Network Consortium funded under Agreement 32509 by the U.S. Department of Energy (DOE), Office of Energy Efficiency & Renewable Energy, Solar Energy Technologies Office (EERE, SETO). This work was authored in part by NREL, operated by Alliance for Sustainable Energy, LLC for the U.S. DOE under contract no. DE-AC36-08GO28308. The views expressed in the article do not necessarily represent the views of the DOE or the U.S. Government. Instruments and materials are identified in this paper to describe the experiments. In no case does such identification imply recommendation or endorsement. The U.S. Government retains and the publisher, by accepting the article for publication, acknowledges that the U.S. Government retains a nonexclusive, paid-up, irrevocable, worldwide license to publish or reproduce the published form of this work, or allow others to do so, for U.S. Government purposes.

References

[1] K. Roy-Choudhury, “Connecting accelerated aging to the field to understand the mechanism of backsheet cracking,” Proc. NREL PV Rel. Work., 2020.

[2] *Y.* Voronko, G.C. Eder, M. Knausz, G. Oreski, T. Koch, K.A. Berger, “Correlation of the loss in photovoltaic module performance with the ageing behaviour of the backsheets used,” Prog. Photovolt. Res. Appl., vol. 23, no. 11, pp. 1501–1515, 2015, doi: 10.1002/pip.2580.

[3] A. Omazic, G. Oreski, M. Edler, G.C. Eder, C. Hirschl, G. Pinter, M. Erceg, “Increased reliability of modified polyolefin backsheet over commonly used polyester backsheets for crystalline PV modules,” J. Appl. Polym. Sci., vol. 137, no. 30, pp. 48899–n/a, 2020, doi: 10.1002/app.48899.

[4] T. Niewelt, J. Schön, W. Warta, S.W. Glunz “Degradation of crystalline silicon due to boron–oxygen defects,” IEEE J. Photovolt., vol. 7, no. 1, pp. 383–398, Jan. 2017, doi: 10.1109/JPHOTOV.2016.2614119.

[5] F. Fertig, F. Kersten, K. Petter, M. Bartzsch, F. Stenzel, A. Mette, B. Klöter, J.W. Müller, “Light and elevated temperature induced degradation of multicrystalline silicon solar cells and modules,” 26th NREL Workshop Cryst. Silicon Sol. Cells Modul., 2016.

[6] “IEC TS 62788-7-2 Measurement procedures for materials used in photovoltaic modules - Part 7-2: Environmental exposures - Accelerated weathering tests of polymeric materials,” Int. Electrotech. Comm., pp. 1–26, Sep. 2017.

[7] A. Sinha, J. Qian, K. Hurst, S.L. Moffitt, L.T. Schelhas, D.C. Miller, P. Hacke, “UV-Induced Degradation of High-Efficiency Solar Cells with Different Architectures,” Proc. IEEE PVSC, 2020, 1990-1991, doi: 10.1109/PVSC45281.2020.9300993..

[8] “IEC 61215-2: Terrestrial photovoltaic (PV) modules - Design qualification and type approval - Part 2: Test procedures,” Int. Electrotech. Comm. Geneva, pp. 1–97, 2016.

[9] “ISO 2813: Paints and varnishes — Determination of gloss value at 20°, 60° and 85°,” Int. Standards. Org. Geneva, pp. 1–23, 2014.

[10] S. Uličná, N.M. Al Hasan, R.L. Arnold, B.H. King, A. Maes, D.C. Miller, J.M. Newkirk, L.T. Schelhas, A. Sinha, K. Terwilliger, M. Thuis, K.V. Durme, “BACKFLIP: Identification of Materials and Changes Upon Aging of Emerging Fluoropolymer-Free and Industry-Benchmark PV Backsheets”, Proc IEEE PVSC, 2021, . Xxx

[11] D.C. Miller, B. Åke-Sultan, A. Borne, R. Eugen, B.L. Givot, J. Jung, S.W. MacMaster, B.K. McDanold, U.H. Nilsson, N.H. Phillips, I.A. Tappan, N.S. Bosco, “The development of a DC breakdown voltage test for photovoltaic insulating materials”, Proc. IEEE PVSC Conf., 2017, 2864-2869.

[12] M. Owen-Bellini, S.L. Moffitt, A. Sinha, A.M. Maes, J.J. Meert, T. Karin, C. Takacs, D.R. Jenket, J.Y. Hartley, D.C. Miller, P. Hacke, L..T. Schelhas, “Towards validation of combined-accelerated stress testing protocols through failure analysis of polyamide-based backsheets,” Sci. Rep, 2021, https://doi.org/10.1038/s41598-021-81381-7.

[13] M. Thuis, N.M. Al Hasan, R.L. Arnold, B. King, A. Maes, D.C. Miller, J.M. Newkirk, L.T. Schelhas, A. Sinha, K. Terwilliger, S. Uličná, K.V. Durme “BACKFLIP: A Comparison of Emerging Non-Fluoro-Based Co-Extruded PV Backsheets to Industry-Benchmark Technologies”, NREL-PR-5K00-80362, 2021, 1-20.

[14] I.S. Khan, J. Morse, R.R. White, D.C. Miller “A custom high-throughput optical mapping instrument for accelerated stress testing of PV module materials,” submitted IEEE J PV, 2021, xxx.

[15] Y. Lyu, A. Fairbrother, M. Gong, J.H. Kim, A. Hauser, G. O'Brien, X. Gu “Drivers for the cracking of multilayer polyamide-based backsheets in field photovoltaic modules: In-depth degradation mapping analysis,” PIP, 2019, 1–13, 2020, https://doi.org/10.1002/pip.3260.

[16] G. Oreski, G.C. Eder, Y. Voronko, A. Omazic, L. Neumaier, W. Mühleisen, G. Ujvari, R. Ebner, M. Edler, "Performance of PV modules using co-extruded backsheets based on polypropylene", SOLMAT, 223, 2021, 110976, doi.org/10.1016/j.solmat.2021.110976.

[17] A. Sinha, V.S.P. Buddha, E.J. Schneller, K.O. Davis, G. TamizhMani “Solder bond degradation of fielded PV modules: Climate dependence of intermetallic compound growth,” Proc. IEEE Conf., 2019, 1393–1397, doi: 10.1109/PVSC40753.2019.8981139.

[18] D.C. Miller, M. Owen-Bellini, P.L. Hacke, “Use of indentation to study the degradation of photovoltaic backsheets,” SOLMAT, 201, 2019, 110082. https://doi.org/10.1016/j.solmat.2019.110082.

[19] F. Rummens, “How to test thermal endurance - depending on backsheet structure,” IEEE TC82 WG2 meeting, Braunschweig, 2019.

[20] B.C. Smith, Infrared spectral interpetation: A systematic approach, CRC Press: New York, 1999.

[21] C.R. Osterwald, "Terrestrial Photovoltaic Module Accelerated Test-to-Failure Protocol", NREL/TP-520-42893, 2008, 1-16.

[22] J. H. Wohlgemuth, D. W. Cunningham, P. Monus, J. Miller and A. Nguyen, “Long term reliability of PV modules,” Proc. WCPEC, 2006, pp. 1942-1946, 2050-2053, doi: 10.1109/WCPEC.2006.279905..

[23] W. Herrmann, N. Bogdanski, “Outdoor weathering of PV modules — Effects of various climates and comparison with accelerated laboratory testing,” Proc. IEEE PVSC, 2011, 002305-002311, doi: 10.1109/PVSC.2011.6186415.

[24] M.D. Kempe, J.H. Wohlgemuth”Evaluation of temperature and humidity on PV module component degradation,” Proc. IEEE PVSC, 2013, 120-125, doi: 10.1109/PVSC.2013.6744112.